IEEE Photonics Journal
An IEEE Photonics Society Publication

Open Access

Unconventional Production of Bright White Light Emission by Nd-Doped and Nominally Un-Doped Y_2O_3 Nano-Powders

Volume 6, Number 4, August 2014

G. Bilir
G. Ozen
J. Collins
M. Cesaria
B. Di Bartolo

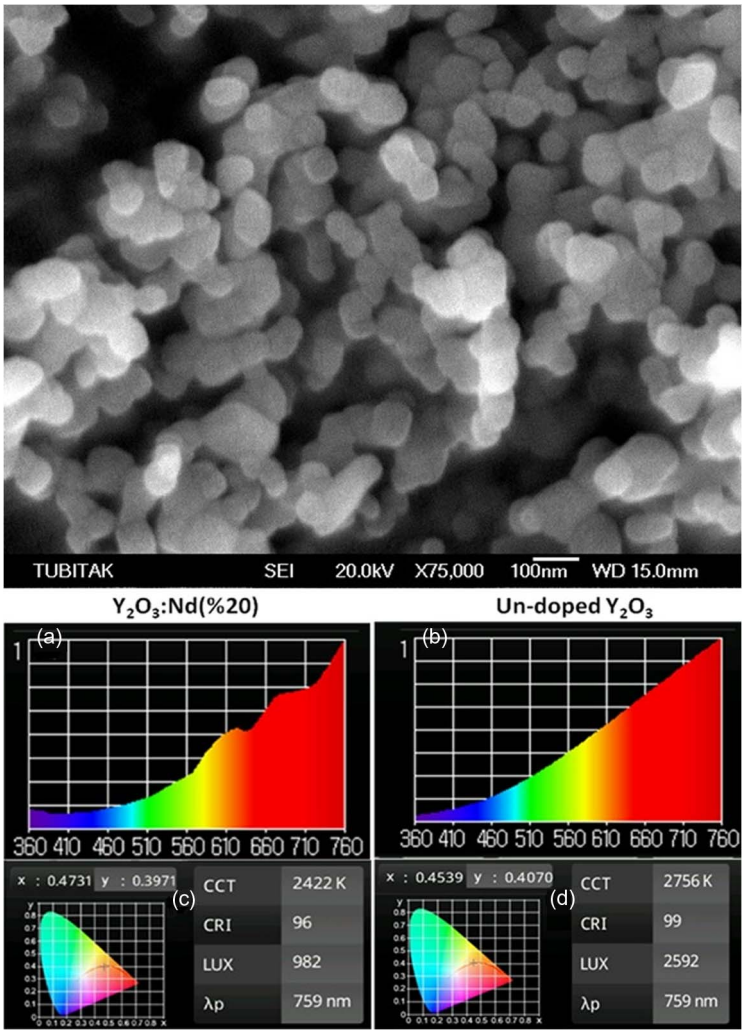

DOI: 10.1109/JPHOT.2014.2339312
1943-0655 © 2014 IEEE

Unconventional Production of Bright White Light Emission by Nd-Doped and Nominally Un-Doped Y_2O_3 Nano-Powders

G. Bilir,[1,2] G. Ozen,[1] J. Collins,[3] M. Cesaria,[4] and B. Di Bartolo[2]

[1]Department of Physics, Istanbul Technical University, Istanbul 34469, Turkey
[2]Department of Physics, Boston College, Chestnut Hill, MA 02467 USA
[3]Department of Physics, Wheaton College, Norton, MA 02467 USA
[4]Department of Physics, Universita del Salento, 73100 Lecce, Italy

DOI: 10.1109/JPHOT.2014.2339312

Manuscript received May 5, 2014; revised July 4, 2014; accepted July 9, 2014. Date of publication July 16, 2014; date of current version August 1, 2014. Corresponding author: G. Bilir (e-mail: bilir@bc.edu).

Abstract: We report the production of a broad band (ranging from 400 to 900 nm) white light following the monochromatic infrared light (803.5 and 975 nm) excitation of both nominally un-doped and Nd^{3+}-doped Y_2O_3 nano-powders, even up to 20% of Nd^{3+} content. Experimental results indicate that such emission feature is a nano-scale phenomenon, cannot be ascribed to an overlap of sharp emission bands in the un-doped case and, even if assisted by the Nd^{34} presence, is a host matrix-related process. The measured white light emission is strongly dependent on either environment pressure (a pressure threshold occurs) or pumping power. The rising patterns of the white light emission were found to increase faster for either increasing Nd^{3+} content and pumping power or decreasing particle size. Notably, high correlated color temperature (2756 K), color rendering index (99), and efficiency (864 lx/W) values were measured for the un-doped sample under 803.5 nm exciting wavelength.

Index Terms: Y_2O_3, white light emission, laser diode, laser spectroscopy.

1. Introduction

Nano-phosphors (nanoscale-sized solid, inorganic crystallites showing luminescence upon excitation) based on rare earth (RE) doped Y_2O_3 are important optical materials, with Y_2O_3 being the best host matrix for RE-dopants due to its chemical and thermal stability, similar ionic radius with respect to RE ions and cut off phonon energy of 380 cm^{-1}. Among optical materials, lanthanide ions have attracted the interest of researchers for their ability to up-convert infrared light to the visible one. Particularly, neodymium (Nd^{3+}) ion, besides being very efficient for solid-state laser applications, is a very good candidate for accomplishing such up-conversion process [1], [2].

Nano-phosphor based lighting is widely used but is suffering a drawback due to the fact that the luminescence spectra do not cover the whole visible light range (380–780 nm), namely a white light (WL) spectrum close to that of the sunshine. Therefore such artificial lighting sources are not optimal for indoor lighting or displaying [3] and the production of WL by engineered luminescence spectra remains an active research field.

Nano-powders doped multiply with lanthanide ions have been found to emit WL. When a near-infrared (NIR) diode laser was used to excite (with high power above a certain threshold)

nano-crystalline insulating powders containing lanthanide ions, a very bright white or yellowish light was observed, corresponding to a strong broad emission band covering almost the whole visible region [4]–[9].

A number of workers have found anti-Stokes wide band emission by exciting nano-crystals of compounds in which Nd^{3+} was one of the dopants [10] or a full stoichiometric part of the system [8], [11], [12].

Strek *et al.* have reported the bright up-converted WL emission from $LiYbP_4O_{12}$ [7], $NdAlO_3$ [8] and $LiNdP_4O_{12}$ [10], [11] nano-crystals under low pressure and infrared (IR) excitation. The production of WL spectrum have also been reported by J. Wang *et al.* by using just lanthanide oxides $(Yb_2O_3, Sm_2O_3, CeO_2)$ [5] and $Yb_3Al_5O_{12}$, $(Yb, Y)_2O_3$ crystals [6]. Sato *et al.* [13], Nolas *et al.* [14], and Zhou *et al.* [15] showed that the RE dopants reduce the thermal conductivity of the YAG, Skutterudites and Lanthanum Zirconate ceramics. Also Roura *et al.* [16], [17] observed broadband emission from SiC nano-particles and mechanically milled Si.

Notably, while the WL production reported in the literature was obtained by materials doubly doped with different RE ions or including RE ions as stoichiometric components, we have observed WL by singly Nd doped and nominally un-doped insulating oxide materials too. In this respect, this paper reports our detailed experimental studies on the broadband "white light" (such nomenclature is supported by the evaluated Commission Internationale de l'Eclarage (CIE) coordinates) emitted following the IR laser-light excitation of Nd-doped Y_2O_3 $(Y_2O_3 : Nd)$ nano-crystals with different Nd concentrations ranging from zero to 20%. Surprisingly, we observed WL even in the nominal absence of Nd dopant in the samples. Moreover no WL was found to be emitted by Nd^{3+}-doped Y_2O_3 bulk crystals.

2. Experimental Details

2.1. Preparation of the $Y_2O_3 : Nd^{3+}$ Nano-Powders

To produce samples of nano-sized Y_2O_3 particles doped with trivalent Nd^{3+}, concentration of 2, 5, 10, and 20% were prepared by thermal decomposition of yttrium-neodymium alginate. Details on the preparation method were described elsewhere [18]–[20]. Briefly, this method is based on the thermal decomposition of alginate gels. In this process yttrium nitrate hexahydrate $Y(NO_3)_3 \cdot 6H_2O$ (99.8%), neodymium nitrate hexahydrate $Nd(NO_3)_3 \cdot 6H_2O$ (99.9%) and low viscosity (250 cps of 2% solution) alginic acid sodium salts with analytical grade are used as starting reagents. The reaction that occurs in thermal decomposition process is given as

$$4\left[Y(NO_3)_3 \cdot 6H_2O\right] \rightarrow 2Y_2O_3 + 6N_2O_5 + 24H_2O.$$

The nano-particles were synthesized at 500 °C and then annealed at 600, 800, 1000, and 1400 °C. The effect of such annealing treatment was to increase the particle size from 50 to 248 nm.

Here-after the Nd^{3+}-doped Y_2O_3 samples will be referred to as $Y_2O_3 : Nd$ (%), where % stands for the corresponding Nd^{3+} doping percentage.

Commercially available Y_2O_3 nano-samples with particle sizes of 20 to 40 nm and with the purity of 99.999% purchased from US Research Nanomaterials, Inc.

2.2. Structural Characterization of the $Y_2O_3 : Nd^{3+}$ Samples

Analysis of the crystal structure of the Nd^{3+}-doped samples was performed by X Ray Diffraction (XRD) patterns. XRD investigations were carried out with a Bruker AXS D8 Model (Cu-Kα radiation) diffractometer at 40 kV and 30 mA setting in the 2θ range from 20° to 70° with scanning steps of 0.02°. The average particle size L of the powders was estimated by using the Scherrer Equation [21]

$$L = \frac{K\lambda}{\beta \cos\theta}$$

where K is a constant varying with the method of taking the breadth ($0.89 < K < 1$, with $K = 0.89$ for spherical particles), λ is the wavelength of the incident X-ray beam, β is the width at half maximum of the XRD peak of a specific lattice plane (hkl) in radians, and θ is the center angle of the considered Bragg reflection (XRD peak by the plane (hkl)).

As a further confirmation of the average particle size, SEM images of the samples were obtained by a JEOL 6335F model scanning electron microscope.

2.3. Emission Characterization

The continuous emission WL spectra were produced by pumping the samples with the output of a Laser Drive Inc. Model LDI-820 laser diode operating at 803.5 nm with the maximum output power of 3 W or of a similar diode operating at 975 nm with the maximum output of 10 W. The signal was directed toward the entrance slit of a 1 m McPherson Model 2051 monochromator and chopped at a frequency of 250 Hz before entering the slit. The monochromator provided a resolution 0.8 Å with the slits set at 50 Å and a wavelength reproducibility of 0.1 Å. The optical signal was detected by HamamatsuR1387 photomultiplier tube with an S20 response, sent to an EG&G Model 5210 lock-in amplifier and recorded in a computer.

Two spectral regions were investigated:

1. a region from 850 to 1500 nm where the emission from the $^4F_{3/2}$ level of Nd occurs;
2. an optical region from 400 to 900 nm where the WL emission occurs.

To perform experiments in the temperature range 30–300 K, the samples were mounted on the cold finger of a closed cycle Helium refrigerator. This system uses a Janis Research Model RD Dewar connected with a Leybold Model RW2 compressor. The temperature of the cold finger was controlled by using a Lake Shore Cryotronics 331 Model temperature controller.

The rise pattern and the decay pattern of the WL were measured by using a shutter that allowed the light to reach its full intensity and then cut sharply the pumping power, operating with a repetition cycle of 10 sec.

The use of the diode operating at 975 nm allowed us to investigate the effect of the exciting wavelength on the WL output of the samples.

An Avantes AvaLight-Hal-Cal calibration light source was used to correct our spectra for the sensitivity of our system.

We had also at our disposal an Allied Scientific Pro ASP-MK350 Model Illuminance Meter that allowed us to measure the International Commission on Illumination (CIE) coordinates, the Correlated Color Temperature (CCT), the Color Rendering Index (CRI), illuminance, and to view the spectrum of the WL. We also measured the above parameters of a 60 W commercial incandescent bulb for comparison.

3. Results

The X-ray diffraction patterns of the as-synthesized Y_2O_3 : Nd samples are shown in Fig. 1 as function of the Nd^{3+} content. The diffraction peaks observed in the XRD-pattern can be indexed to cubic phase Y_2O_3 (JCPDF: 25/1200); no other phase was detected. The observed diffraction peaks correspond to the Bragg diffraction from the (211), (222), (400), (411), (332), (431), (440), (532), (622), and (613) planes. Only the (hkl) values of the most prominent peaks are indicated in the XRD pattern with the strongest peak observed at $2\theta = \sim 29.5^\circ$ corresponding to the plane (222) for all the samples. The room temperature lattice parameter of the unit cell of the yttria cubic phase estimated by the XRD patterns was 10.6051 Å which was in good agreement with the JCPDS database of pdf number 83–0927. Notably, as the Nd^{3+} concentration increases from 2% to 10%, the prominent diffraction peaks become sharper and more intense thus suggesting a refinement of the sample crystallinity and/or increased nano-powder sizes. One would expect that an increase of the Nd^{3+} ion concentration would lead to peaks with slightly broader width and reduced intensity, but the observed results agree with report according to which a Nd^{3+} dopant may act as an heterogeneous nucleation and crystallization site [22] and improve the

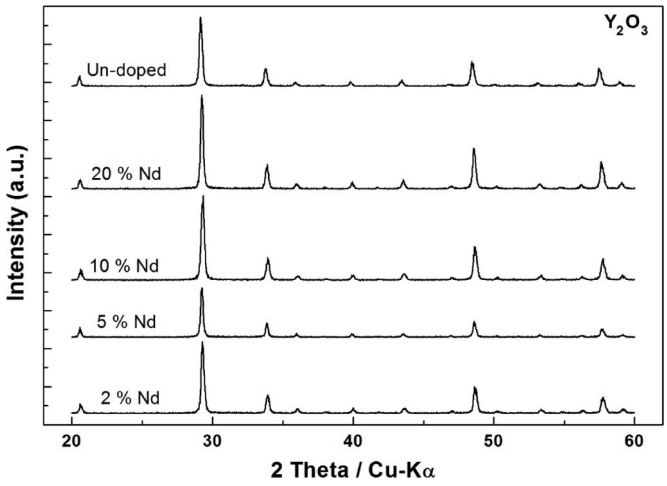

Fig. 1. XRD patterns of the samples.

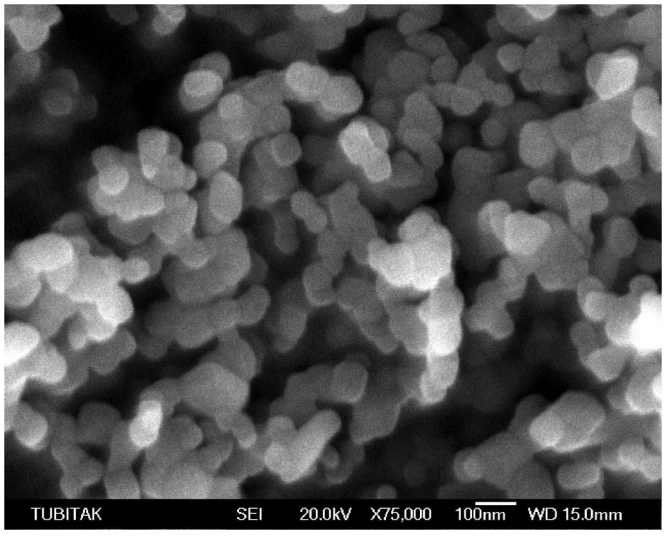

Fig. 2. Representative SEM image of the Y_2O_3 : Nd (2%).

sample crystallinity. On the other hand, doping-induced microstrain and local distortion of the host lattice structure due to the difference in the ionic radii between the Y host cation (0.9 Å) and Nd^{3+} dopant (0.980 Å) are expected effects because of the relevant doping level of our samples. The crystallite size of the samples, calculated by the Debye-Scherrer formula applied to the diffraction feature (222), resulted to be in the range 25–250 nm according to the synthesis and annealing temperatures. The SEM image of the 2% Nd^{3+} doped Y_2O_3 spherical nanoparticles are shown in Fig. 2.

3.1. Results of the 803.5 nm Excitation

Turning to the emission properties of the Y_2O_3 : Nd samples excited by the 803.5 nm wavelength, the IR spectrum consists of three groups of spectral lines due to the $^4F_{3/2} \rightarrow {}^4I_{9/2}$, $^4I_{11/2}$, and $^4I_{13/2}$ transitions. The general aspect of the spectra was found to be similar for Nd^{3+} content ranging up to 10%. Notably for Nd^{3+} concentration of 10% it is not possible to see any

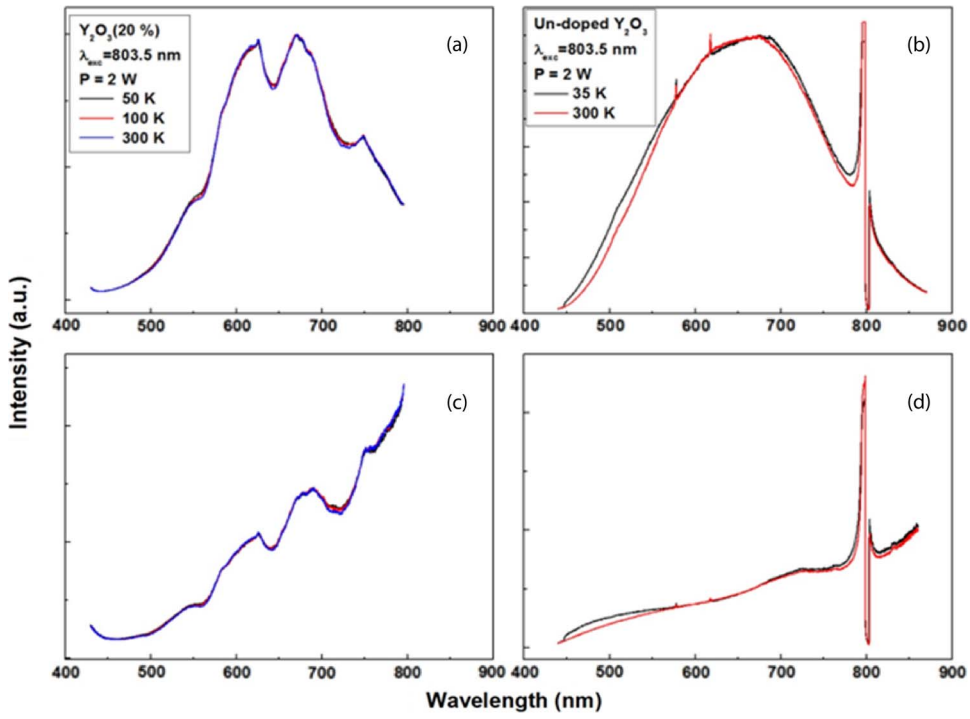

Fig. 3. Environment temperature dependence and the general aspect of the WL spectrum under 803.5 nm excitation, (a) uncorrected spectrum of 20% Nd^{3+} doped sample, (b) uncorrected spectrum of un-doped sample, (c) corrected spectrum of 20% Nd^{3+} doped sample for system response, and (d) corrected spectrum of un-doped sample for system response.

Nd-related IR emission in bulk crystals; this is an indication that the concentration at which the luminescence quenches is higher in the nano-powders than in the crystal [23].

Since the IR emission of the $Y_2O_3 : Nd^{3+}$ systems was already investigated in our previous papers [18], [19], it will not be considered further. Instead, in the present paper our attention will be focused on the WL band accompanying the IR emission of our samples as a function of the Nd^{3+} dopant content.

In this regard, Fig. 3(a) and (b) show the WL spectrum collected in the 400–900 nm wavelength range of the samples $Y_2O_3 : Nd$ (20%) and $Y_2O_3 : Nd$ (0%), corresponding to the highest (20%) and lowest (0%) Nd^{3+} content, respectively, under excitation at 803.5 nm with pumping power of 2 W and various environment temperatures. Some of our preliminary results on WL emitted by infrared excited un-doped metal oxide nano-powders have been reported elsewhere [24], [25]. The WL spectra under examination were emitted by samples with crystallite size of 26 nm. The spectrum of the doped sample consists of a wide band with three dips associated with the absorption of the Nd^{3+} ion (the 803.5 nm wavelength matches with the strong absorption of the Nd^{3+} ions in this region). The three dips due to the absorption of Nd^{3+} can clearly be seen in the measured spectrum (see Fig. 3(a)), the corrected spectrum (see Fig. 3(c)) and the spectrum measured by using the illuminance meter (see Fig. 4(a)). There is also a good agreement between Figs. 3(d) and 4(b), corresponding to the spectrum corrected and measured by using the illuminance meter, respectively, of the un-doped sample.

The parameters CCT, CRI, illuminance, and Commission Internationale de l'Eclarage (CIE) coordinates of the WL emitted by both doped and un-doped samples under examination are shown in the corresponding figures (see Fig. 4(a) and (b)) and summarized in Table 1.

It was observed that both CCT and CRI

i) decrease turning from the un-doped to the doped sample;

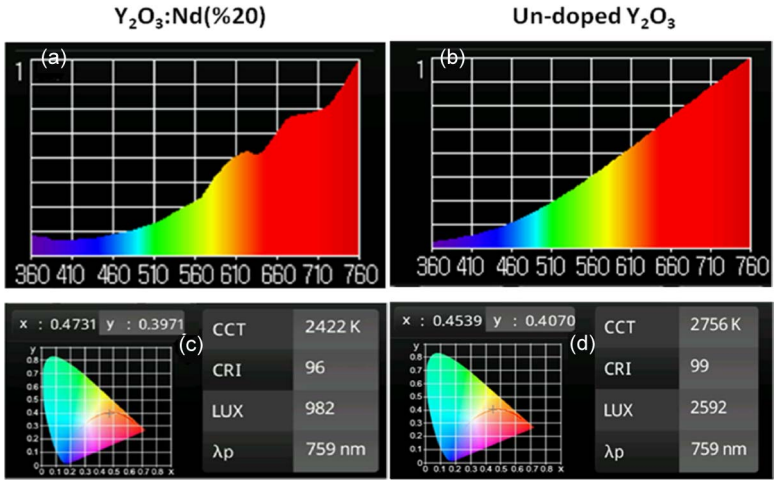

Fig. 4. (a) Measured spectrum of 20% Nd^{3+} doped sample by using illuminance meter, (b) measured spectrum of un-doped sample by using illuminance meter, (c) CIE coordinates and the measured CCT, CRI values for 20% Nd^{3+} doped sample, and (d) CIE coordinates and the measured CCT, CRI values for un-doped sample.

TABLE 1

Summary of results when using 803 nm excitation

Sample	CIE	CCT	CRI	Efficiency
Y_2O_3:Nd (20%)	x = 0.47 y = 0.39	2422 K	96	327 lum/W
Un-doped Y_2O_3	x = 0.45 y = 0.40	2756 K	99	864 lum/W
Incandescent Lamp (60 W)	x = 0.46 y = 0.41	2666 K	99	636 lum /W

ii) depend on the pumping power: while the CCT value goes up, CRI was found to go down with decreasing pumping power:
iii) depend on the environmental pressure around the sample: while the CCT value goes up, CRI was found to go down with increasing environmental pressure.

In regard to point i), the reduction of CCT and CRI upon increasing Nd content could be ascribed to the strong absorption of the Nd ions clearly observable from Fig. 3.

One important CIE Standard Illuminant is the color point A, located in the CIE color space by the coordinates (0.448, 0.408) and also called warm white point with CCT of 2856 K. This point marks the chromaticity of tungsten incandescent lamps, namely the artificial light sources most comfortable for human eye. Accounting for the lighting standards, we also compared the performance of our samples with the one of a 60 W incandescent lamp (see Fig. 5 and Table 1). Notably, the CIE coordinates, CCT and CRI values of our obtained WL emission are very close to those of a commercial incandescent bulb source: CRI approaching the theoretical limit (100) and CCT closer to the warm white point were measured for the un-doped sample. Moreover, as a power excitation of 3 W was used for the 803.5 nm pumping diode, the efficiency of the WL emitted by our samples seems to be better than the one of the incandescent lamp source (see Table 1).

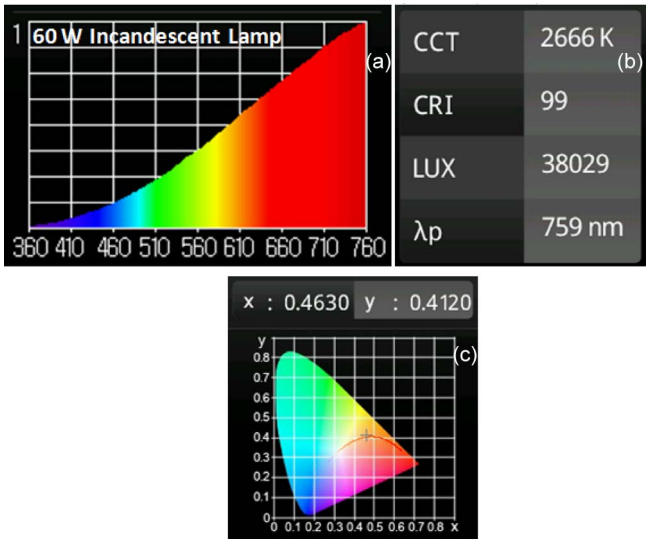

Fig. 5. (a) Measured spectrum; (b) CCT, CRI, and illuminance values; and (c) CIE coordinates of a commercial 60 W incandescent bulb obtained by using illuminance meter.

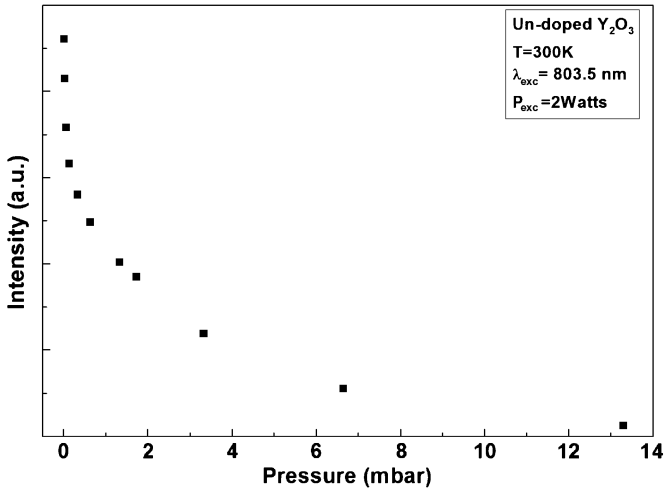

Fig. 6. Pressure dependence of the WL intensity in nominally un-doped Y_2O_3.

WL emission from commercially available 99.999% pure Y_2O_3 nano-powders was also obtained under both of 803.5 nm and 975 nm laser diode excitation. The general aspects of the WL emission from commercial Y_2O_3 were found to be the same as the ones observed for our synthesized samples.

The investigation of the WL dependence on the nature and pressure of the background gas revealed that while it was easy to obtain WL under low pressure, it was possible to obtain WL at atmospheric pressure by increasing the pumping power. In this respect, as Fig. 6 shows for the un-doped sample with the crystalline size of 26 nm, the WL intensity falls down rapidly upon increasing the background pressure. Fig. 6 is representative, since the same behavior is shown by Nd^{3+}-doped samples. The threshold value of the pumping power to obtain WL under 0.02 mbar pressure was found to decrease with increasing dopant concentration: 0.7 and 0.12 W for nominally un-doped and heavily doped materials, respectively. We were also able to detect WL at atmospheric pressure, and in such a case, the threshold power value was 0.73 and 1.1 W for the 20%

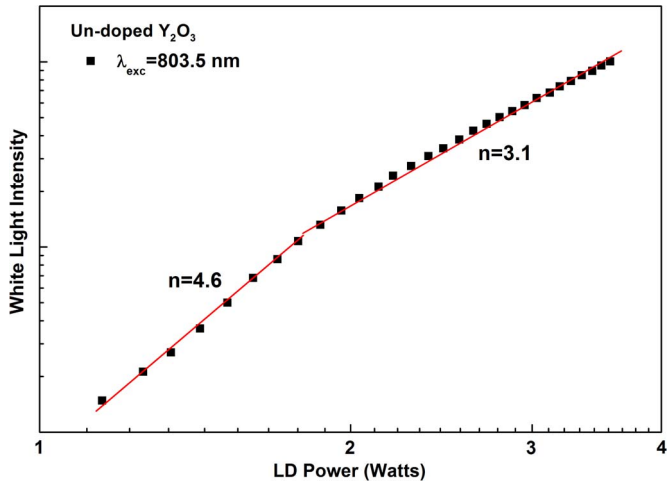

Fig. 7. WL intensity variation with pumping power in nominally un-doped Y_2O_3.

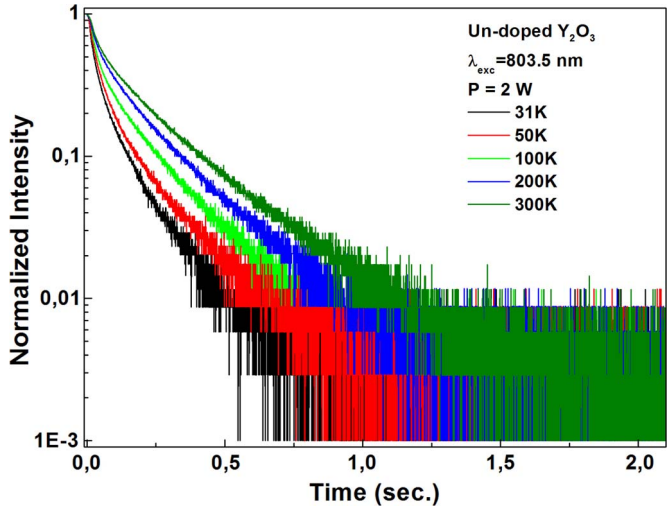

Fig. 8. Dependence of decay patterns on environment temperature in nominally un-doped Y_2O_3.

Nd^{3+} doped and the nominally un-doped sample, respectively. Such findings indicate that the presence of the Nd^{3+} ions makes easier to induce WL.

Tests dealing with the nature of the background gas were also performed. After filling the evacuated sample chamber with nitrogen (N_2), quenching of the WL was observed. Similar results were observed by using helium (He), another inert gas. All of the performed checks indicate that the WL is sensitive to the pressure of the gas present in the sample chamber, as long as this gas is inert.

The changes in the WL intensity with pumping power in an un-doped sample with 26 nm crystalline size (see Fig. 7) demonstrate that WL intensity "I" varies with the pumping power "P" according to the law $I = P^n$, n being an exponent depending on either the exciting wavelength or the laser diode pumping power (LD Power). As the fit results in Fig. 7 indicate, the exponent n is found as 3.1 and 4.6 by linear fitting for two different linear regions of the experimental data.

In order to further characterize the WL we measured its rise pattern and decay pattern, counting on such parameters being more sensitive to the conditions of measurements and to the

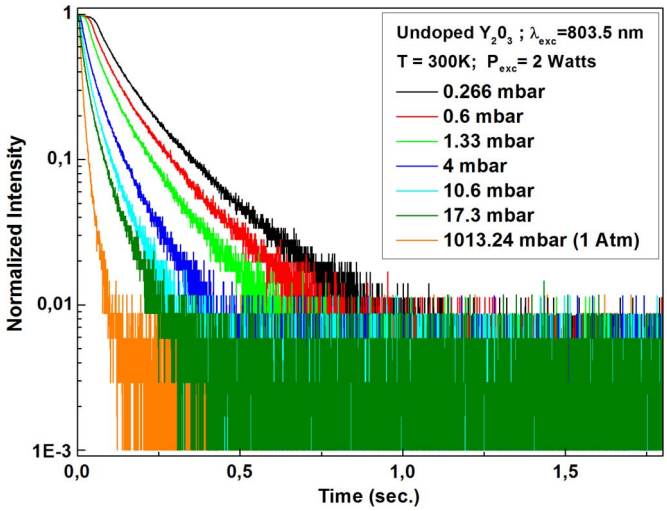

Fig. 9. Variation of decay patterns with environment pressure in nominally un-doped Y_2O_3.

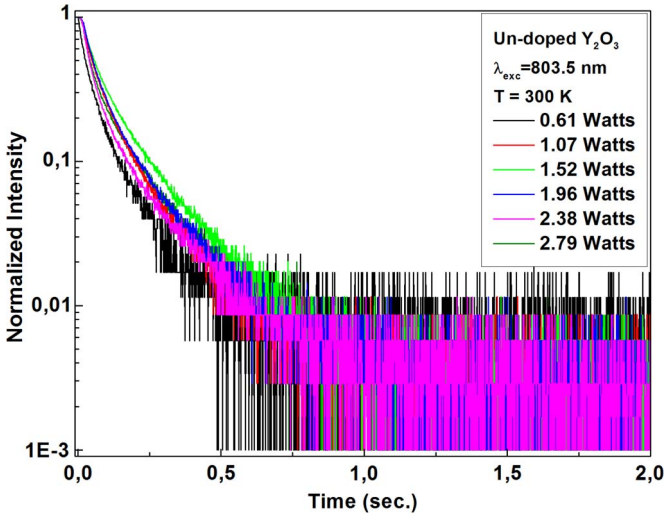

Fig. 10. Dependence of decay patterns on pumping power in nominally un-doped Y_2O_3.

composition of the samples. We summarize our experimental findings concerning the WL emitted by the un-doped sample as follows.

i) The decay patterns of the un-doped Y_2O_3 were found to be sensitive to the temperature of the sample holder, as shown in Fig. 8.
ii) The decay patterns were found to be very sensitive to the environment pressure showing faster falling down with increasing pressure (see Fig. 9).
iii) The decay patterns and rise patterns vs. the pumping power shown in Figs. 10 and 11, respectively indicate that, while no significant pumping power-dependence of the WL decay patterns occurs, the rising patterns are very sensitive to the pumping power, becoming shorter with increasing pumping power.

Considering the results on the Y_2O_3 : Nd (20%) sample, Fig. 12 reports that the WL spectrum changes in intensity and in detail by changing the diode pumping power: the dips due to absorption by the Nd^{3+} ions progressively disappear with increasing pumping power and the emission intensity is enhanced by increasing the pumping power. Such experimental findings suggest mechanisms of filling/saturation of the dopant energy levels.

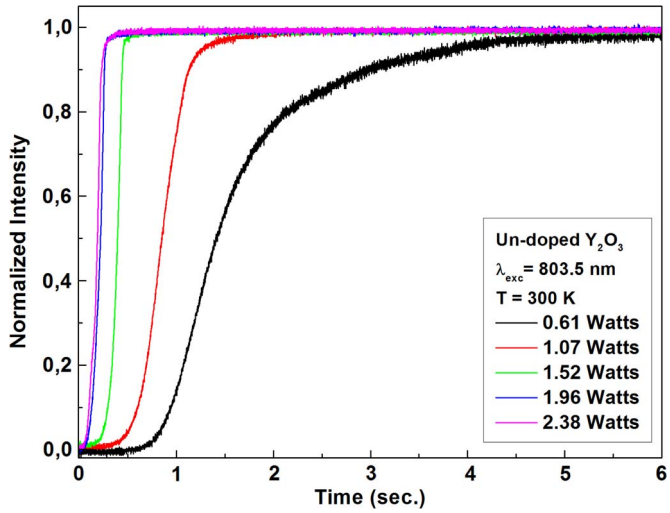

Fig. 11. Rise pattern dependence on pumping power in nominally un-doped Y_2O_3.

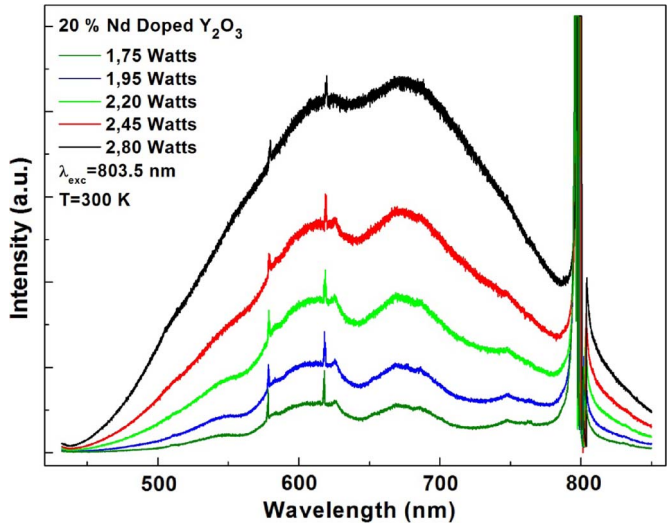

Fig. 12. Pumping power dependence of the WL spectrum in 20% Nd^{3+} doped Y_2O_3 with crystalline size of 26 nm.

In addition to the result in Fig. 12, our measurements showed the following:

i) The decay patterns did not vary sensibly with Nd^{3+} concentration (see Fig. 13), thus suggesting that the WL decay is mainly a host-dependent effect.
ii) The onset of the WL strongly depends on Nd^{3+} concentration with a delay before the rise of the WL to its maximum value longer with decreasing Nd^{3+} content (see Fig. 14).
iii) The decay patterns associated with the Y_2O_3 : Nd (10%) sample plotted vs. particle size show that while no difference is observable in the 20 to 50 nm size range, the pattern corresponding to 250 nm decays more slowly (see Fig. 15).

The rise pattern behavior of the Y_2O_3 : Nd (10%) sample depends on the particle size, namely it decreases and becomes steeper with decreasing particles size (see Fig. 16).

3.2. Results of the 975 nm Excitation

Turning to the laser diode operating at 975 nm, once again WL was observed when exciting the samples with such a source. The acquired spectrum was corrected for the sensitivity of the

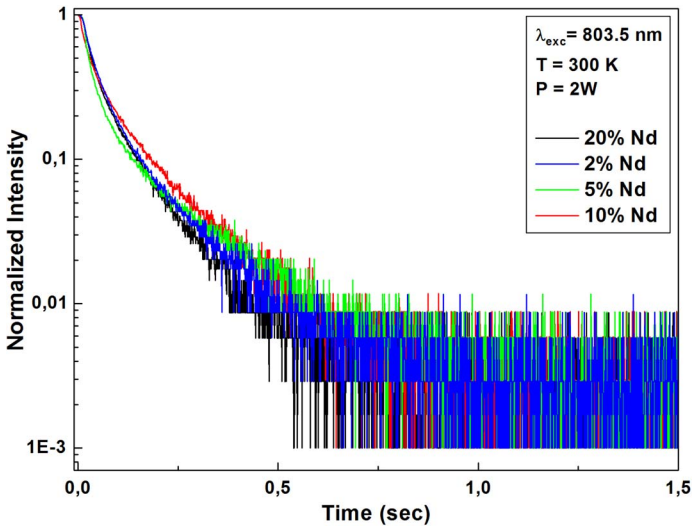

Fig. 13. WL decay patterns variation with the Nd^{3+} concentration.

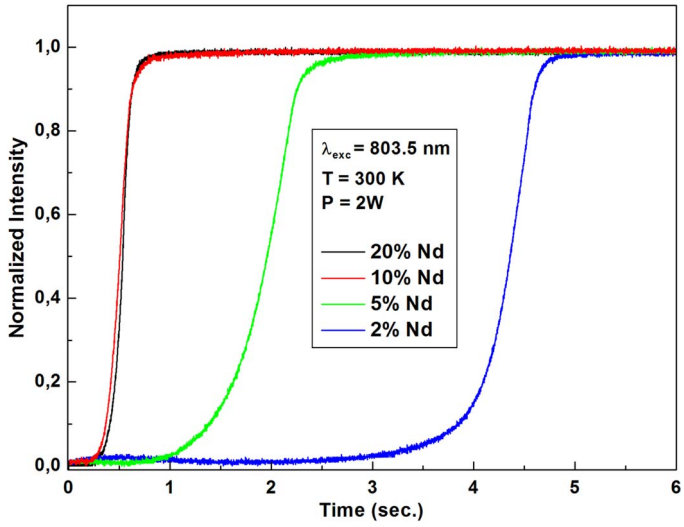

Fig. 14. Rise pattern dependence on Nd^{3+} concentration.

apparatus and also measured by using the illuminance meter for both doped and un-doped samples. We also measured the spectrum of the un-doped sample after the excitation at various times with time interval between successive measurements of 10 min.

The following was inferred by our experiments.

i) The general aspect of the broadband WL spectrum was similar to the one obtained by using the 803.5 nm exciting source (see Fig. 17) with a red-shift of the peak position up to 50 nm.

ii) The threshold pumping power value was 6 W at 0.02 mbar.

iii) A pressure value as low as 0.02 mbar was sufficient to obtain WL, and no WL was detectable under atmospheric conditions.

iv) The corrected spectra and those measured by the illuminance meter (see Fig. 18) look similar and are in good agreement both for doped and un-doped samples.

v) While measuring the emission of the un-doped samples in 10 min steps, a blue-shift of the emission peak was observed (see Fig. 19) and, moreover, the intensity was found

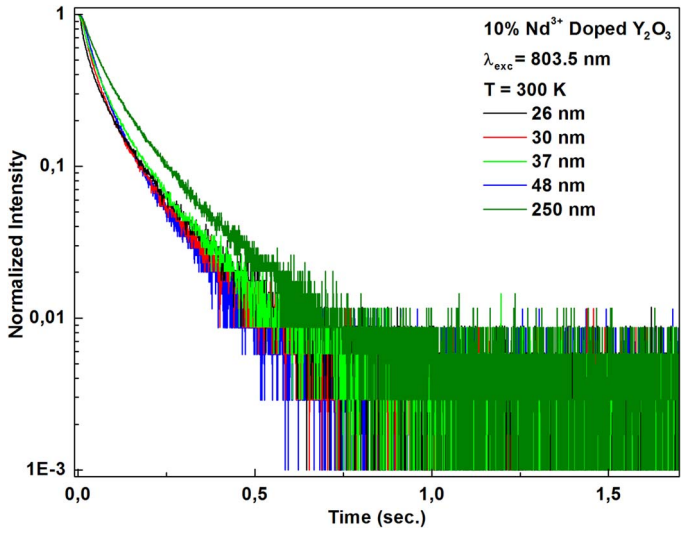

Fig. 15. Dependence of decay patterns on powder size in 10% Nd^{3+} doped Y_2O_3.

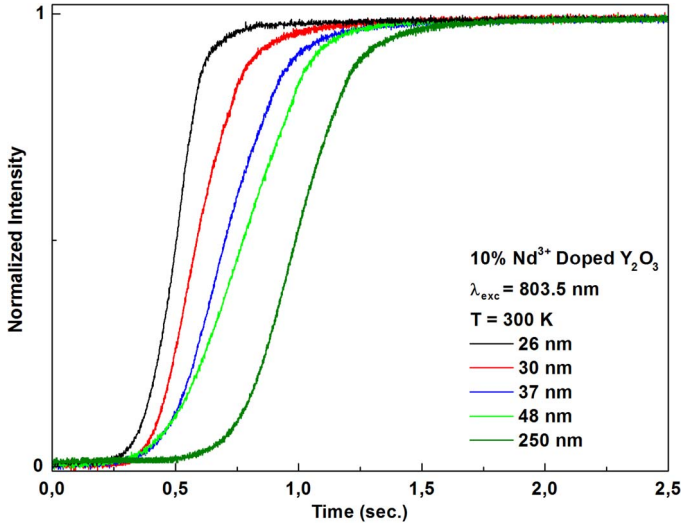

Fig. 16. Rise pattern dependence on powder size 10% Nd^{3+} doped Y_2O_3.

to increase 8 times with time and the spectrum became stable after five successive measurements. The amount of the shift was 15 nm, which corresponds to temperature change 77 K according to Wien Displacement Law.

vi) With regard to the observed pumping power-dependence of the WL spectrum, with increasing pumping power an intensity change and a blue-shift of 19 nm of the WL spectrum were detected (see Fig. 20).

vii) The intensity variation with pumping power under 975 nm excitation, shown in Fig. 21, indicated a strong dependence of the WL emission on this power.

viii) All the decay patters were found to be non exponential, as observed in all previously examined cases.

Turning to the sample characterization according to the lighting standards parameters, CIE coordinates, CCT, CRI and illuminance of the WL emitted from doped and un-doped samples under 975 nm excitation were measured. The results are given in Fig. 18(a) and (b) and summarized in Table 2.

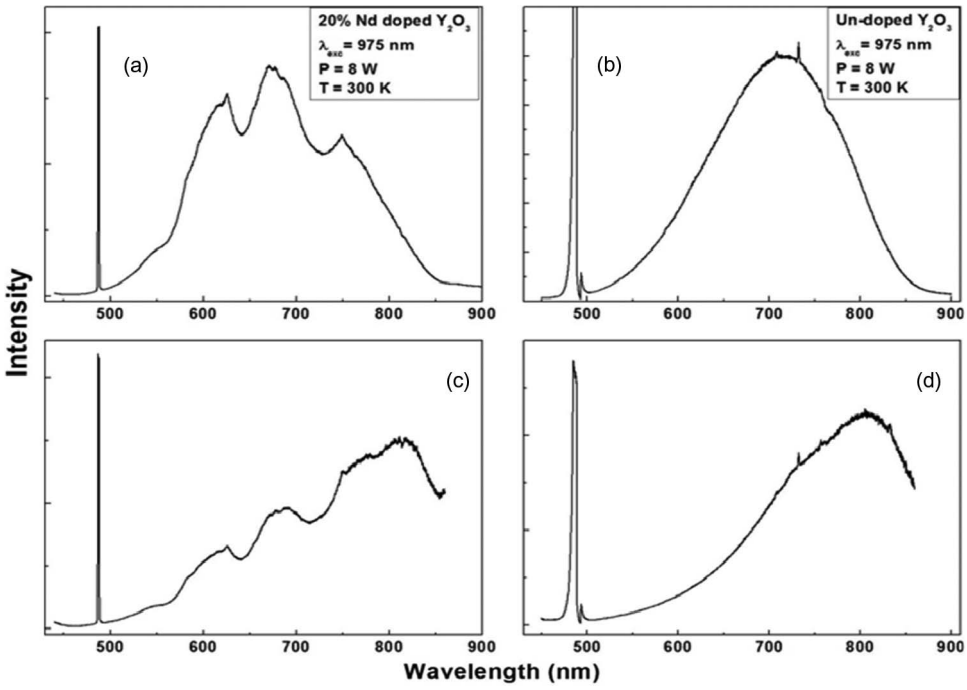

Fig. 17. General aspect of the WL spectrum under 975 nm excitation (a) uncorrected spectrum of 20% Nd^{3+} doped sample, (b) uncorrected spectrum of un-doped sample, (c) corrected spectrum of 20% Nd^{3+} doped sample for system response, and (d) corrected spectrum of un-doped sample for system response.

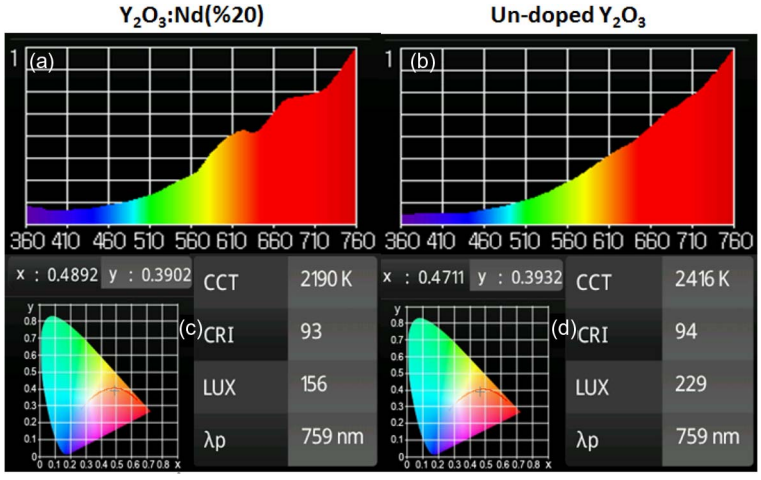

Fig. 18. (a) Measured spectrum of 20% Nd^{3+} doped sample by using illuminance meter, (b) measured spectrum of un-doped sample by using illuminance meter, (c) the CIE coordinates and the measured CCT, CRI values for 20% Nd^{3+} doped sample, and (d) the CIE coordinates and the measured CCT, CRI values for un-doped sample.

Notably, as already observed under 803.5 nm excitation source, both of CCT and CRI values were found to decrease with the presence of the dopant. However, the same samples exhibited a better WL performance under the 803.5 nm than under the 975 nm excitation. Moreover, a dependence on either the pumping power or environment pressure was observed for both CCT and CRI in the case under examination (975 nm excitation). In detail, while CCT goes up, the CRI value was found to go down with decreasing (increasing) pumping power (environment pressure).

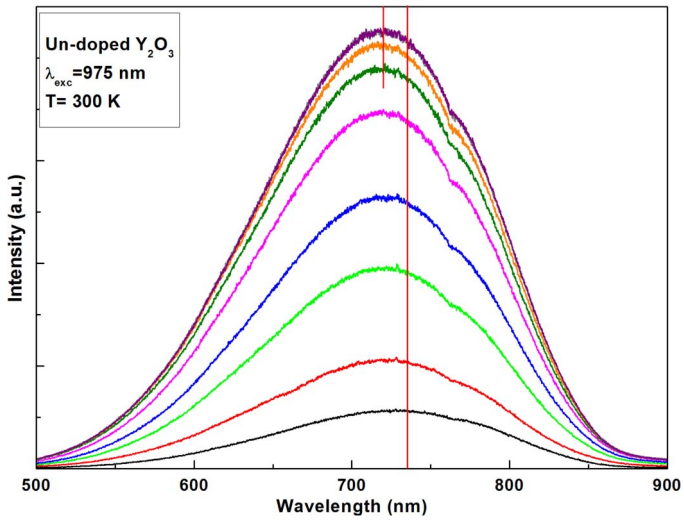

Fig. 19. The change of the WL spectrum under 975 nm excitation. The curves correspond to measurements made subsequently every 10 min, starting from the lowest curve and moving upward.

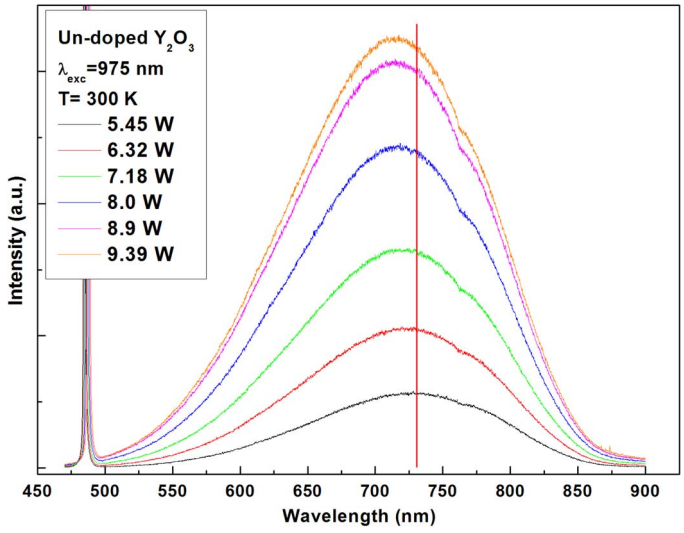

Fig. 20. The change of the WL spectrum with changing pumping power of 975 nm laser diode.

As a further result, WL emission from commercially available 99.999% pure Y_2O_3 nanopowders was also obtained under both of 803.5 nm and 975 nm laser diode excitation. The general aspects of the WL emission from commercial Y_2O_3 were found to be the same as the ones observed for our synthesized samples.

4. Discussion of the Results

The amount of experimental results of our experiments demands careful consideration of their general aspects. The following basic observations can be made.

1. Since no WL emission was observed by bulk samples of Nd^{3+} doped Y_2O_3 exposed to the same exciting infrared light as the nano-particle samples, definitely the observed production of WL can be considered as typical of the nanoscale regime.
2. The spectral distribution of the WL is to a large extent independent on the Nd^{3+} concentration and even the presence of the Nd^{3+} dopant. While Nd occurrence favors the WL

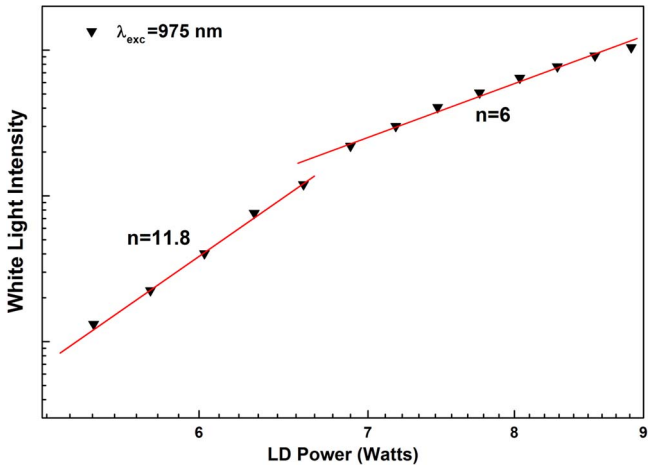

Fig. 21. Power dependence of the WL intensity under 975 nm excitation.

TABLE 2

Summary of results when using 975 nm excitation

Sample	CIE	CCT	CRI	Efficiency
Y_2O_3:Nd(20%)	x = 0.49	2190 K	93	19.5 lum/W
	y = 0.39			
Un-doped Y_2O_3	x = 0.47	2416 K	94	28.6 lum/W
	y = 0.39			

generation but is not necessary to induce such process, the presence of Nd makes it easier to obtain WL emission under low pumping power and higher environment pressure conditions.

3. The temperature of the sample's holder does not influence the spectral shape and seemingly the intensity of the WL emission.
4. The pressure in the sample environment has a great influence on the intensity of the WL. It acts in the opposite sense with respect to the intensity of the exciting infrared light: low pressure favors the emission of WL, and a strong excitation does likewise. The latter occurrence is expected: more exciting light results in greater absorption and consequently in a stronger emission. The former effect, the influence of pressure, needs a more elaborate explanation. As nano-crystalline Y_2O_3 is very hygroscopic, adsorption of water on the nano-particle surface is very likely [26], [27], which could contribute to the absorption of the pumping wavelengths, adsorbed water molecules easily evaporate with decreasing environment pressure, even at room temperature, and due to the excitation-induced warming up effect. Hence, surface adsorption of H_2O could contribute to the absorption of the infrared radiation at high atmospheric pressure, because H_2O has a relatively broad absorption band peaking at 760 nm and at 800 nm its absorption coefficient is 0.02 cm^{-1} [27]. The pressure dependence of the WL intensity indicates the occurrence of de-excitation mechanisms. As the nature of the gas-nano-particle interaction is not chemical when inert gases are considered, at given pressure conditions, the fact that the WL intensity is lower in the presence of light inert gases indicates the effective role of the collision density. Therefore, the pressure dependence of the WL intensity can be accounted for adsorption of polar species on the nano-particle surface as well as scattering effects gas-nano-particle causing

de-excitation and/or heating dissipation. In this regard an alternative or concurrent pressure-dependent de-excitation mechanism can be invoked based on the thermal conductivity of the nano-powders. This parameter is enhanced by the ambient pressure and reduced when this pressure is lowered. At low pressures the crystallites are more isolated from each other and from the cold finger and can reach higher temperatures favoring the emission of WL.

5. Of particular interest is Fig. 12 which shows the WL spectrum of the 20% Nd^{3+} doped Y_2O_3 sample with dips corresponding to the Nd^{3+} absorption. The dips become shallower as the excitation power increases, as a consequence of the saturation of the Nd^{3+} absorption at high excitation power. Consequently the absorption process seems to receive the dominant contribution from the host material rather than from Nd-based processes.
6. The characterization of the spectral properties and of the processes taking place in the nano-systems must include the investigation of such dynamical characteristics as the patterns related to the rise of the WL intensity following the sudden excitation by the infrared radiation and the decay pattern that follow the sudden interruption of such a radiation. In this regard we may say that, as expected, the dynamical parameters are remarkably sensitive to the variation of such experimental conditions as temperature of the samples (see Fig. 8), pressure of the samples' environment (see Fig. 9) or dimension of the powder crystallites (see Fig. 16). One expected outcome of the measurements of the decay patterns of the WL is their independence of how much energy was stored in the system (see Fig. 10).
7. The most noticeable aspect of the decay patterns is their deviation from exponentiality. Such behavior could be inferred by the role played by the powders' surfaces, role that becomes more important as the radius of the particle is reduced. Going from the surface to the center of a particle one would encounter a variety of conditions, with each condition determining a different decay patterns. The observed pattern is the superposition of the various different patterns. Accordingly the deviation from an experimental pattern is in general more pronounced in smaller particles.
8. The spectral distribution of the detected WL resembles very closely the one of an incandescent lamp, which is still unmatched with respect to its color quality, meaning inherent resembling the sun light which is the most comfortable for human perception. We have demonstrated the possibility to obtain WL with very high efficiency and CRI approaching the theoretical limit with an alternative approach. Our experimental results make our WL emission very interesting at both fundamental and applicative levels and open the way to an alternative route with respect to incandescent lamps.

The following considerations deal with occurrences that manifest themselves in different ways depending on the wavelength of the exciting infrared light.

1. The WL spectrum produced by the 975 nm excitation is not significantly different form that produced from the 803.5 excitation. The dependence of the WL intensity on the fourth power of the exciting 803.5 nm diode power suggests the multi-photon aspect of the absorption process. In fact, an interpretation of the exponent n occurring in the law $I = AP^n$ is just in terms of number of photons in multi-photon absorption events. The same can be inferred in the case of the other exciting wavelength (975 nm). However, being a 975 nm photon less energetic than an 803.5 nm photon, more photons are required to induce multi-photon absorption in the un-doped system. This is indeed the case: the WL intensity was found to be proportional to a higher exponent n of the power of the exciting 975 nm source (see Fig. 21).
2. The decay patterns following the 975 nm excitation are not significantly different than those following the 803.5 nm excitation, as one would expect. The different experimental conditions may produce different amount of excitation, but this should have no effect on the enfolding of the spontaneous decay.
3. The wavelength of excitation has a greater influence on the rise patterns than on the decay patterns. A most notable effect is produced by the 975 nm excitation on the rise patterns, by which the WL intensity reaches its maximum value. Fig. 19 is illustrative in this regard.

In it we can see that it took about one hour for the WL intensity to reach its maximum intensity. Fig. 20 represents a similar behavior obtained by exciting the sample with increasing power of the 975 nm light, confirming that the pattern represented in Fig. 19 reflect a gradual absorption of the exciting infrared light. Such an occurrence is indeed, to our best knowledge, never seen before.

4. The important thing to notice is that the wavelength of the exciting infrared light has an effect on the time it takes the system to fully absorbs this light. For practical applications wavelengths like 975 nm would have to be avoided and attention should be given to a proper choice of the infrared wavelengths that would ensure a prompt absorption response.

5. Conclusion

We have presented some experimental results concerning the emission of WL by Nd^{3+} doped and, very importantly, nominally un-doped Y_2O_3 nano-particles under different conditions of excitation. Our study was directed toward the investigation of the basic parameters controlling the onset and build-up of the observed WL and its decay following the sudden cut-off of the exciting light. We found that the presence of Nd as an optically active dopant in the nano-particles favored the production of the WL, but was not essential for this production.

Another important parameter was the pressure in the sample environment: low pressure favored the emission of the WL. However, we found that under appropriate conditions WL emission could be obtained even at atmospheric pressure. This last result points to the potential applications of systems like the one we examined to the field of lighting.

Acknowledgement

G. Bilir would like to thank the Support Branch for Research Projects of Istanbul Technical University (BAP).

References

[1] R. Balda *et al.*, "Infrared-to-visible upconversion in Nd^{3+} doped chalcohalide glasses," *Phys. Rev. B.*, vol. 64, pp. 144101-11–144101-18, 2001.
[2] D. L. Russell and K. Holliday, "Upconversion and energy transfer dynamics in $Nd^{3+}:KLiYF_5$," *Opt. Commun.*, vol. 191, no. 3–6, pp. 277–294, May 2001.
[3] S. Pimputkar, J. S. Speck, S. P. DenBaars, and S. Nakamura, "Prospects for LED lighting," *Nat. Photon.*, vol. 3, pp. 180–182, 2009.
[4] S. Redmond, S. C. Rand, X. L. Ruan, and M. Kaviany, "Multiple scattering and nonlinear thermal emission of Yb^{3+}, $Er^{3+}:Y_2O_3$ nanopowders," *J. Appl. Phys.*, vol. 95, no. 8, pp. 4069–4077, 2004.
[5] J. Wang and P. A. Tanner, "Upconversion for white light generation by a single compound," *J. Amer. Chem. Soc.*, vol. 132, no. 3, pp. 947–949, 2009.
[6] J. Wang, J. H. Hao, and P. A. Tanner, "Luminous and tunable white-light upconversion for YAG (Yb3Al5O12) and (Yb,Y)2O3 nanopowders," *Opt. Lett.*, vol. 35, no. 23, pp. 3922–3924, 2010.
[7] W. Stręk *et al.*, "White emission of lithium ytterbium tetraphosphate nanocrystals," *Opt. Exp.*, vol. 19, no. 15, pp. 14083–14092, 2011.
[8] W. Stręk, L. Marciniak, D. Hreniak, and A. Łukowiak, "Anti-stokes bright yellowish emission of NdAlO3 nanocrystals," *J. Appl. Phys.*, vol. 111, no. 2, pp. 024305, 2012.
[9] R. K. Verma and S. B. Rai, "Continuum emission in Nd^{3+}/Yb^{3+} co-doped $Ca_{12}Al_{14}O_{33}$ phosphor: Charge transfer state luminescence versus induced optical heating," *Chem. Phys. Lett.*, vol. 559, pp. 71–75, 2013.
[10] L. Marciniak, W. Strek, A. Bednarkiewicz, A. Lukowiak, and D. Hreniak, "Bright upconversion emission of Nd^{3+} in $LiLa_{1-x}Nd_xP_4O_{12}$," *Opt. Mater.*, vol. 33, no. 10, pp. 1492–1494, 2011.
[11] W. Strek *et al.*, "The effect of pumping power on fluorescence behavior $LiNdP_4O_{12}$ nanocrystals," *Opt. Mater.*, vol. 33, no. 7, pp. 1097–1101, 2011.
[12] T. S. Atabaev, Y. Hwang, and H. Kim, "Color-tunable properties of Eu^{3+}- and Dy^{3+}-codoped Y_2O_3 phosphor particles," *Nanoscale Res. Lett.*, vol. 7, pp. 556, 2012.
[13] Y. Sato, J. Akiyama, and T. Taira, "Effect of rare-earth doping on thermal conductivity of $Y_3Al_5O_{12}$ crystals," *Opt. Mater.*, vol. 31, no. 5, pp. 720–724, 2009.
[14] G. S. Nolas, G. A. Slack, D. T. Morrelli, T. M. Tritt, and A. C. Ehrlich, "The effect of rare-earth filling on the lattice thermal conductivity of skutterudites," *J. Appl. Phys.*, vol. 79, no. 8, pp. 4002–4008, 1996.
[15] H. Zhou and D. Yi, "Effect of rare earth doping on thermo-physical properties of lanthanum zirconate ceramic for thermal barrier coating," *J. Rare Earth*, vol. 26, no. 6, pp. 770–774, 2008.

[16] P. Roura and J. Costa, "Radiative thermal emission from silicon nanoparticles: A reversed story from quantum to classical theory," *Eur. J. Phys.*, vol. 23, no. 2, pp. 191–203, 2002.
[17] P. Roura *et al.*, "Blackbody emission from nanostructured materials," *J. Lumin.*, vol. 80, no. 1–4, pp. 519–522, 1999.
[18] G. Bilir, G. Ozen, J. Collins, and B. Di Bartolo, "Synthesis and spectroscopy of nanoscale $Y_2O_3 : Nd^{3+}$ phosphors," *ECS Trans.*, vol. 50, no. 41, pp. 1–7, 2013.
[19] G. Bilir, G. Ozen, J. Collins, and B. Di Bartolo, "Fabrication and spectral investigation of $Y_2O_3 : Nd^{3+}$ nanoparticles," *Appl. Phys. A*, vol. 115, no. 1, pp. 263–273, 2014.
[20] H. Kaygusuz, G. Bilir, F. Tezcan, F. B. Erim, and G. Özen, "Biopolymer-assisted synthesis of yttrium oxide nanoparticles," *Particuology*, vol. 14, pp. 19–23, 2014.
[21] P. Scherrer, "Bestimmung der größe und der innerenstruktur von colloid teilchenmittels röntgen strahlen," *Göttinger-Nachrichten Gesell.*, vol. 2, pp. 98–100, 1918.
[22] W. Liu, H. Wang, S. Zhan, and W. Li, "Splitting and the broadening of the emission bands of $Y_2O_3 : Eu^{3+}$,Nd^{3+} and its dependence on Nd^{3+} concentration and annealing temperature," *J. Mater. Sci.*, vol. 46, no. 23, pp. 7620–7625, 2011.
[23] X. Hou, S. Zhou, T. Jia, H. Lin, and H. Teng, "Effect of Nd concentration on structural and optical properties of $Nd : Y_2O_3$ transparent ceramic," *J. Lumin.*, vol. 46, no. 9, pp. 1953–1958, 2011.
[24] G. Bilir and B. Di Bartolo, "Production of bright, wideband white light from Y_2O_3 nano-powders induced by laser diode emission," *Opt. Mater.*, vol. 36, no. 8, pp. 1357–1360, 2014.
[25] G. Bilir and J. Liguori, "Laser diode induced white light emission of $\gamma - Al_2O_3$ nano-powders," *J. Lumin.*, vol. 153, pp. 350–355, 2014.
[26] F. Vetrone, J. C. Boyer, J. A. Capobianco, A. Speghini, and M. Bettinelli, "Luminescence spectroscopy and near-infrared to visible upconversion of nanocrystalline $Gd_3Ga_5O_{12} : Er^{3+}$," *J. Phys. Chem. B*, vol. 107, no. 39, pp. 10 747–10 752, 2003.
[27] J. A. Curcio and C. C. Petty, "The near infrared absorption spectrum of liquid water," *J. Opt. Soc. Amer.*, vol. 41, no. 5, pp. 302–304, 1951.